Single Superparamagnetic Bead Detection and Direct Tracing of Bead Position Using Novel Nanocomposite Nano-Hall Sensors

Mihai S. Gabureac, Laurent Bernau, Giovanni Boero, and Ivo Utke

***Abstract*—We show that nanocomposite materials consisting of superparamagnetic nanoparticles embedded in a matrix are very good candidates for a novel generation of Hall nanosensors with high spatial and magnetic resolution, capable of detecting superparamagnetic beads suspended at different heights on top of the sensor. Two detection schemes were used: 1) *static*—the bead was centered on top of the sensor and detected with a combination of ac and dc orthogonal magnetic fields, and 2) *dynamic*—using nanomanipulation in an electron microscope for moving the bead precisely at different heights above the sensor and using only one magnetic field (ac). The Hall sensors were directly written by focused-electron-beam-induced deposition and the active area was refined by focused ion beam milling. A magnetic field resolution of about 300 μT(Hz)$^{-1/2}$ and a spatial resolution of 230 nm(Hz)$^{-1/2}$ were measured. Both resolutions could be improved by at least an order of magnitude with the suppression of the parasitic inductive signals.**

***Index Terms*—Hall effect, magnetic materials, nanocomposites, nanoscale devices.**

I. Introduction

NANOCOMPOSITE materials consisting of magnetic particles embedded in a matrix are good candidates for Hall sensors with high spatial and magnetic resolution because they have an enhanced magnetic sensitivity (giant Hall effect) [1]–[3] and their active area can be as small as a few tens of nanometer, without loss of magnetic sensitivity [4]. The down-scalability of this type of material is the main advantage with respect to the more sensitive 2-D electron gas semiconducting Hall sensors that have an active area limited in the micrometer range by charge depletion effects, which drastically decrease their magnetic flux resolution [5], [6]. With respect to pure ferromagnetic materials that exhibit the extraordinary Hall effect [7], [8], the nanocomposite Hall sensors have one or two order of magnitude higher sensitivities and are linear in the zero magnetic field, when the size of the magnetic nanoparticles is below the superparamagnetic limit. The low field linear behavior and the high saturation fields of this superparamagnetic material are also the advantages with respect to the magnetoresistive sensors [9].

We used focused-electron-beam-induced deposition (FEBID) [10] to deposit the functional nanocomposite material. FEBID shows great potential as it is a direct-write nanodevice prototyping technique and enables prototyping of a wide variety of materials, shapes, and related nanosensors and nanodevices, like strain sensors [11], scanning probes [12]–[14], single electron transistors [15], magnetic logic [16], magnetic domain transport [4], polarization gratings on telecom lasers [17], and nanochannels in membranes [18]. Our nano-Hall sensor focused electron beam (FEB) deposits consist of superparamagnetic cobalt nanocrystals of a few nanometers in size, separated by a carbonaceous matrix. Depending on the size and interdistance of the nanocrystals, deposits with the same composition (atomic concentration of metallic nanoparticles) can have different electrical conductivities [19] and magnetic sensitivities [20], [21].

Here, we show that our nano-Hall sensors are capable of detecting a single superparamagnetic bead (Dynabead M280 from Dynal, 2.8 μm in diameter). Such beads, coated with streptavidin and DNA or proteins, are routinely used as biomolecular magnetic labels in biomedical research for studying enzymatic DNA processes, like winding/unwinding, copying, and transcription [22]–[24]. Anchoring the DNA/bead ensemble to a magnetic sensor will enable lab-on-chip studies of such processes [25].

II. Sensor Fabrication

A. FEBID of Nanocomposite Co–C Hall Nanosensors

The Hall sensors were fabricated by FEBID using cobalt carbonyl $Co_2(CO)_8$ and hydrocarbons from the background pressure as precursors [26]. Si substrates with a 200-nm-thick thermally grown SiO_2 layer were used. Cr–Au electrodes (Cr 10 nm, Au 90 nm thick) were lift-off prepatterned using standard UV and e-beam lithography and e-beam evaporation in a physical vapor deposition (PVD) chamber from Mantis Deposition Ltd.

FEBID was performed in a tungsten gun equipped Hitachi 3600 SEM with a background pressure of $1{\cdot}10^{-5}$ mbar, and a beam energy and current of 25 keV and 1 nA, respectively. An Alemnis gas injection system was used to supply the molecules inside the SEM chamber, close to the e-beam position. The

Manuscript received December 19, 2012; revised March 11, 2013 and May 23, 2013; accepted June 1, 2013. Date of publication June 6, 2013; date of current version September 4, 2013. This work was supported by the EC FP6 project BioNanoSwitch under Grant 043288, the Helvetic Confederation by projects of CTI 10710.1 PFNM-NM and SBF C11.0138, and the COST NanoTP Action MP0901. The review of this paper was arranged by Associate Editor E. Tutuc.

M. S. Gabureac, L. Bernau, and I. Utke are with the EMPA, The Swiss Federal Laboratories for Material Science and Technology, 3602 Thun, Switzerland (e-mail: Mihai.Gabureac@mat.ethz.ch; lbernau@gmx.ch; Ivo.Utke@empa.ch).

G. Boero is with the Ecole Polytechnique Federale de Lausanne, 1015 Lausanne, Switzerland (e-mail: Giovanni.Boero@epfl.ch).

Color versions of one or more of the figures in this paper are available online at http://ieeexplore.ieee.org.

Digital Object Identifier 10.1109/TNANO.2013.2266733

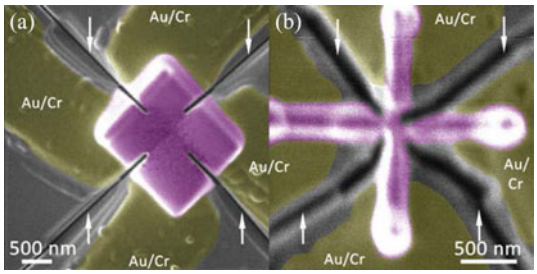

Fig. 1. SEM images of the Hall sensors deposited by FEBID between Cr and Au electrodes: (a) $2 \times 2.5\ \mu m^2$ rectangle, and (b) 200 nm wide lines. The FIB milling (indicated by arrows) allows reducing the active area without decreasing the magnetic sensitivity.

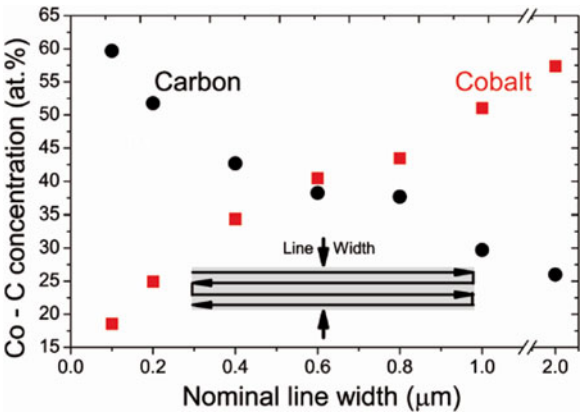

Fig. 2. Cobalt concentration versus the width of 20 μm long Co-FEBID lines on Au, for a 1 nA, 25 keV beam, 2 μs/pixel dwell time, 4 nm pitch, 10 C/cm^2 dose, 1×10^{-5} mbar pressure, and 776 ms refresh time. The inset shows the line scan.

sensors shown in Fig. 1 were deposited with a serpentine scan (see the inset in Fig. 2) and an overall dose of 20 C/cm^2 for the rectangle and 10 C/cm^2 for the cross lines. In either design, the resulting deposit is a nanocomposite material of Co nanocrystals embedded in a carbonaceous matrix.

The Co–C ratio in the rectangle design [see Fig. 1 (a)] could be tuned in the electrical conductive regime between 50 and 70 at.% Co, by changing the beam pulse time [26]. For line deposits shown in Fig. 1(b), energy dispersive X-ray measurements show that the line width additionally influences the Co–C ratio, see Fig. 2. This is due to nonnegligible surface diffusion of hydrocarbons across the deposit rims for small deposit sizes (line widths). Since the composition of submicron deposits is influenced both by the beam pulse time and the deposit width, which are acting like two coupled parameters [27], it can be difficult to achieve the optimum Co concentration for narrow lines as shown in Fig. 1(b), when large hydrocarbon contributions are present as background gas or as surface contamination.

Two types of sensors were produced, as shown in Fig. 1, with the active sensing area refined by focused ion beam (FIB) milling. This approach allowed using large FEBID deposits, as shown in Fig. 1(a), thus avoiding additional size effects on composition aforementioned.

TABLE I
ROOM TEMPERATURE CHARACTERISTICS OF THE FEBID HALL SENSORS WITH RESPECT TO MEASURED SENSITIVITY S_I, AND CALCULATED MAGNETIC FIELD RESOLUTION $B_{\min}$ AND MAGNETIC FLUX RESOLUTION $\Phi_{\min}$ AT THE SENSOR RESISTANCE THERMAL NOISE LIMIT. $\Phi_0 = 0.5$ h/e, THE MAGNETIC FLUX QUANTUM

Sensor shape	Cross (this paper)	Rectangular (this paper)	Cross Ref. [30]
Co_xC_{1-x} (at.%)	65	75	65
Area (nm x nm)	600x600	500x500	100x100
$S_I(\Omega T^{-1})$	0.091	0.036	0.15
$B_{\min}$ (nT Hz$^{-1/2}$)	800	1400	1000
$\Phi_{\min}/\Phi_0$	1.4e-4	1.7e-4	4.5e-6

B. FIB Milling

The active area of the FEBID Hall sensor was refined by Ga^+-FIB milling [28] in a TESCAN VELA FIBSEM; for the square deposit shown in Fig. 1(a), the active size was 600 nm, and for one cross deposit shown in Fig. 1(b), a size smaller than 100 nm was achieved. Such small sizes allow us to constrain the number of beads which can be placed on the sensor [29]. The lateral implantation of Ga was minimized by using very small ion currents at 10 pA at 30 kV. The alignment of cuts was performed with the integrated FIB lithography software which allows defining milling patterns directly on scanned images. Preliminary halo cut experiments showed that after the FIB milling procedure, a two times larger current could be passed through all the Hall sensors tested, before thermal drift was observed. This is probably due to a better thermal conductivity due to the Ga^+ ions implanted in the SiO_2 insulating layer. Furthermore, FIB milling resulted in an increase in the resistance of both types of sensors, confirming the reduction of the size of the active area.

C. Sensor Specifications

The sensor specifications can be tuned via the Co_xC_{1-x} concentration and the active area. Specifications are summarized in Table I for three sensors: two sensors from which bead detection results will be presented in this paper and one sensor from a previous article of ours [30] having a better magnetic flux resolution than published work on semiconductor-based Hall sensors, see [20] and [30].

III. SINGLE SUPERPARAMAGNETIC BEAD DETECTION

The static bead detection was carried out using the method described by Besse *et al.* [31], in the configuration with both external magnetic fields applied perpendicular to the sensor surface. This method allows the detection of the presence of a superparamagnetic bead placed statically on the sensor, by reading a difference in the ac Hall voltage when a larger external dc field is turned ON and OFF. An alternative way to unambiguously detect the presence of the bead is the use of a gradiometry setup as proposed by Mihajlovic *et al.* [32], where two inversely biased Hall sensors are used to measure the magnetic signal of a bead placed on one of the sensors. Almost all other

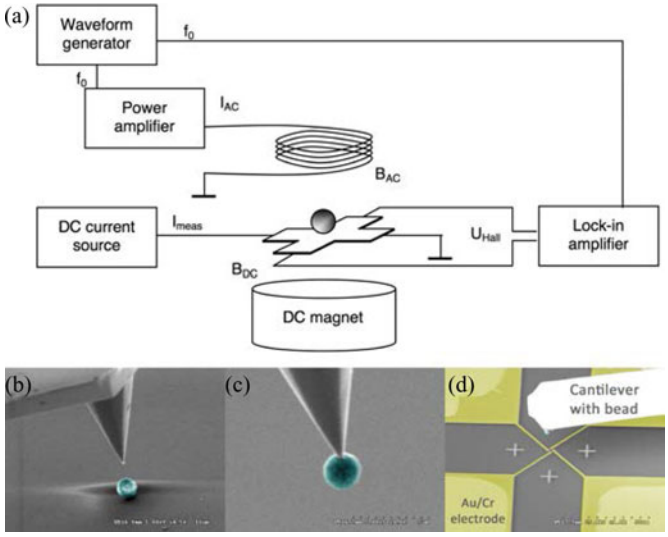

Fig. 3. (a) Schematics of the static bead detection: the dc field is varied by changing the gap between the permanent magnet and the sensor; the ac field is generated with a coil placed above the substrate. (b)–(d) Pick-up of superparamagnetic bead (diameter 2.8 μm) and placing it onto the sensor by nanomanipulation in an SEM.

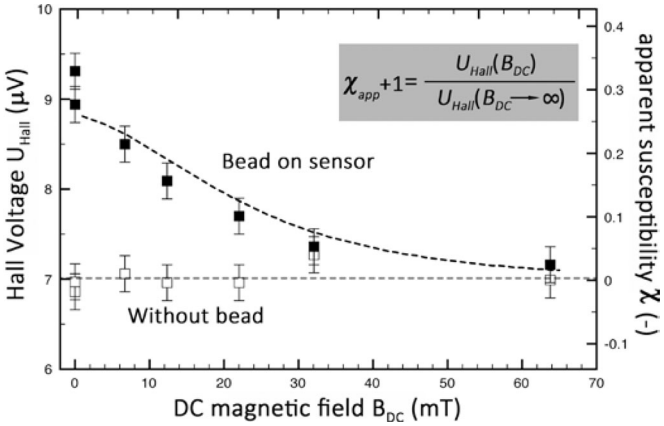

Fig. 4. Hall voltages for different values of the dc field using a 4 mT ac field: comparison of the sensor without bead and with bead placed on the sensor. The maximum contribution of the bead is given at the zero dc field and its value depends on the value of the applied ac field. The inset gives the formula for the apparent susceptibility reported on the second y-axis; $U_{\rm Hall}(B_{\rm dc} \to \infty)$, defined in [31] and [35], was taken as the Hall voltage value measured at saturation.

contributions for the detection of single beads [33], [34] follow these two approaches.

The detection scheme is shown in Fig 3. If a superparamagnetic bead is present on the sensor, the dc field will polarize the magnetic moments changing the total magnetization that generates the ac signal. If the dc field is large enough to saturate the bead, its magnetization will no longer follow the small ac field and the ac Hall signal will be the same as if no bead is present, provided there is no cross-talk between the two magnetic fields and that the sensor response is linear for all fields applied.

We have used a permanent magnet as a technical solution for generating the dc field and varied the distance between the magnet and the sample to obtain a variable dc field. The ac field was generated by a homemade inductive coil with 1000 loops driven at 2 A. In order to account for any nonlinearity of the FEBID sensor in the dc field range, we first measured the dc field by a commercial Hall sensor for each position of the permanent magnet. Then, we measured the Hall voltage generated by the FEBID Hall sensor, placed at the same position as for the predetermined dc fields, first without bead (around 8 mT) and then with bead. Bead placement was accomplished with cantilever-based nanomanipulation and nanopositioning as shown in Fig. 3(b)–(d).

The difference in the ac Hall voltage between the two configurations is plotted in Fig. 4 for discrete values of the dc magnetic bias. As expected, when the dc field is strong enough to saturate the bead magnetization, the weaker ac field is not able to turn the magnetization anymore and the bead becomes magnetically invisible. The signal was measured on the lock-in amplifier (LIA, EG&G 7260); the inductive part of the signal can be separated from the Hall signal by performing first a measurement without a dc bias current in the Hall device, i.e., $I_{\rm meas} = 0$, because of the $\pi/2$ phase difference between the Hall and the inductive signal. The maximum ac Hall signal related to the presence of the bead is obtained with a zero dc field. As shown in Fig. 4, for a Dynabead M-280 with 2.8 μm diameter centered on the surface of the sensor, we typically applied dc fields in the range of a few tens of millitesla, and ac fields of one order of magnitude lower.

In order to eliminate drift problems, we removed the bead and, then, validated the measurements by checking if the same base level as that at the beginning was obtained. This routine also automatically compensates for eventual variations of the Hall voltage due to the nonperfect linearity in the dc field range used, although this should not be the case for the Co–C Hall sensors because of their high saturation fields (around 1 T).

Although this method clearly allows detecting single paramagnetic beads, the vertical ac field configuration has the disadvantage of creating large inductive voltages that add up to the Hall signal and limit the input range on the LIA. In our case, because the ac field was generated by a large coil on the top of our printed circuit board setup, the magnetic flux varied on a macroscopic scale generating inductive signals a few orders of magnitudes larger than the Hall voltage. Since both signals are measured with the same scale on the LIA, we had to reduce the ac frequency below 200 Hz, in order to reduce the induced voltage while still being above the corner frequency for the $1/f$ noise, to make possible the Hall voltage detection. Fig. 4 shows the measured ac Hall voltage as a function of the applied dc field with an ac field of 8 mT. The cross-shaped Hall sensor was used, see Table I. The Hall voltage due to the bead is about 2 μV over a background signal of about 7 μV. The sensing current was $I_{\rm meas} = 10$ mA, the Hall sensor's sensitivity $S_I = 91$ mV/AT, active area was 600×600 nm^2, and its resistance was 34.6 Ω. The apparent susceptibility in Fig. 4 allows making an upper bond estimate of the magnetic susceptibility of the bead at the zero dc magnetic field. Using the Langevin description for the magnetic moment of the superparamagnetic bead [31], [35], it can be calculated to $\chi = 0.7$ (Langevin coefficient $\alpha = 115$ Am^{2}J^{-1}). This value, together with the value $\chi = 0.6$ found by the dynamic measurements (see Section IV below), corresponds well

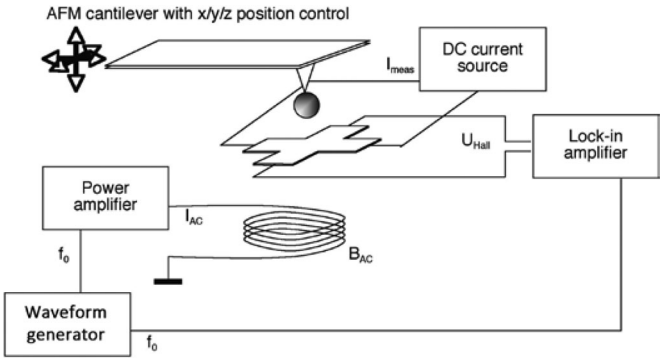

Fig. 5. Principle of the dynamic detection: ac field generated by the bottom coil, bead suspended and moved on AFM cantilever above the sensor.

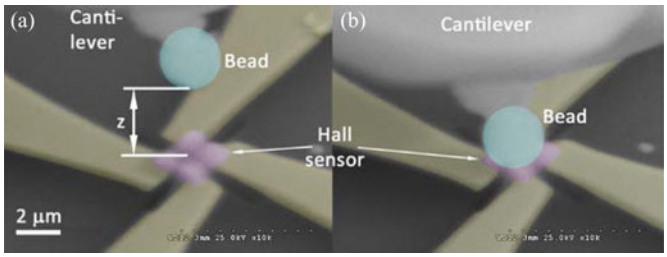

Fig. 6. SEM tilt view of a superparamagnetic bead fixed on a cantilever tip and centered above the Co–C FEBID Hall sensor shown in Fig 1(a). (a) At about $z = 4.5$ μm, and (b) at about 450 nm distance above the sensor.

with the value $\chi = 0.5$ found by vibrating sample magnetometer measurements [36].

IV. Dynamic Single Superparamagnetic Bead Detection

We used the nanopositioners inside the SEM to precisely place the bead attached to the cantilever above the Hall sensors and a single ac magnetic field perpendicular to the sensor, also generated inside the SEM by the homemade magnetic inductive coil as shown in Fig. 5. Since the bead can be *in situ* removed from the sensor (see Fig. 6), one can separate the two Hall contributions: by removing the bead we measured the background Hall signal from the ac field (separated from the inductive signal) which can then be subtracted from the extra signal provided by the bead at a given position above the sensor.

The main advantage of this novel SEM-integrated cantilever approach is that it allows moving and detecting the bead in 3-D, at varying *x*–*y*–*z* positions [37]. This mimics the situation in biological experiments where such beads (lifted by a magnetic field gradient) are fixed by DNA strings above the sensor in microfluidic channels and where changes in z are induced by restriction enzymes curling up the DNA string [22], [23].

We started verifying the diamagnetic nature of the cantilever without bead; within the experimental detection noise of our setup (10 nV), we could not measure any influence on the Hall voltage due to movement of the bare cantilever. Then, we proceeded with the detection of a bead attached to the top of the cantilever, as shown in Fig. 6.

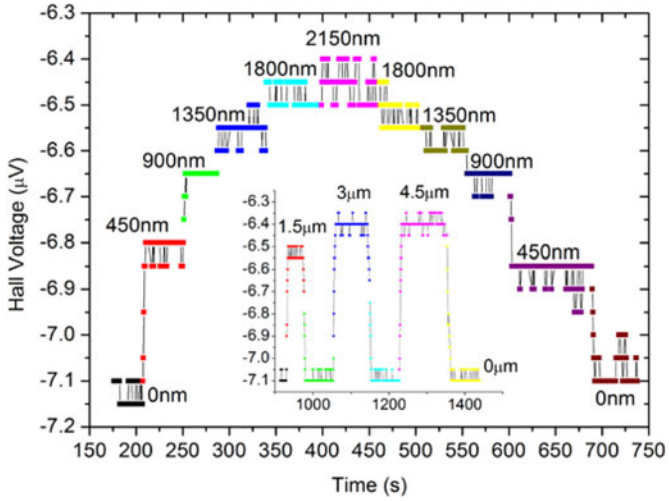

Fig. 7. Variation of the Hall voltage with time when the bead is moved above the sensor (z is indicated). The maximum detection height is 2.1 μm; the largest Hall voltage change is 300 nV when the bead is close to the sensor. The inset shows the Hall voltage when the bead is moved up and down for distances of 1.5, 3, and 4.5 μm.

The variation of the Hall voltage with the position of the bead centered on the top of the sensor ($x = y = 0$) and moved at different heights z above the active area is shown in Fig. 7. For this experiment, the rectangular-shaped sensor was used, see Table I and Fig. 1(a).

The resolution in z (minimum variation in height that produced a measurable change in the Hall voltage using a time constant of 1 s with an equivalent bandwidth of 0.167 Hz) depends on the height of the bead [see (1)]. The main parameter that limited the z-resolution was the large inductive signal with respect to the low Hall signal produced by the superparamagnetic bead (compared to a noise level of 100 nV). At an ac field frequency of 17 Hz ($1/f$ corner frequency was about 10 Hz), we measured a magnetic field resolution of 20 μT(Hz)$^{-1/2}$ without an inductive signal; using the dynamic detection setup, the large inductive signal limited the magnetic field resolution to 300 μT(Hz)$^{-1/2}$ for this sensor.

As can be seen in Fig. 7, the Hall voltage measured with the bead centered on the surface was about 7.1 μV, while the signal with the bead far from the sensor was about 6.4 μV. This gives an effective Hall signal of about 700 nV, with a noise level around 100 nV. For comparison, the inductive voltage was about 450 μV and the sensitivity scale on the LIA was set to 500 μV, with the minimum detectable voltage of 10 nV using the expand option. The dynamic measurements were carried out at 17 Hz, with a dc current of $I_{\mathrm{meas}} = 15$ mA and an ac field of 12 mT. The sensor had a resistance of 35.6 Ω, an active area of around 500×500 nm^2, and a Hall sensitivity of $S_I = 36$ mV/AT. Above a height of 1.8 μm, it was not possible to separate the movement in z, which defines the maximum detection range. Smaller bead position changes can be better detected if the bead is closer to the sensor, as this will give a higher change due to the stray magnetic field of the bead. The Hall voltage U_{Hall} depends on

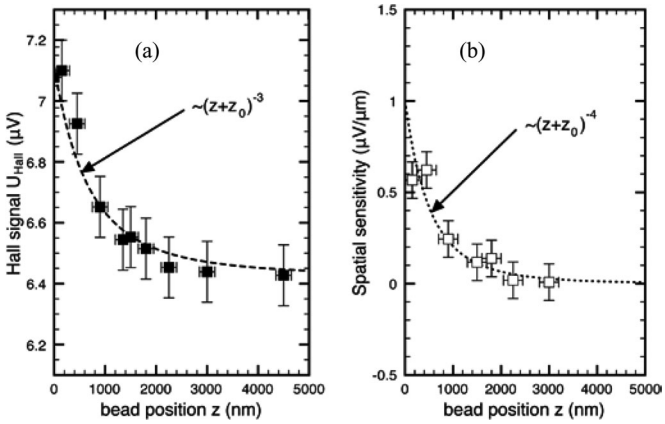

Fig. 8. (a) Hall voltage versus bead distance from values of Fig. 7. The error bar in the Hall signal is the standard deviation from repeated measurements at the same height. (b) Spatial sensitivity derived from (a). Note that z denotes the gap between the bead and sensor as shown in Fig. 6.

the bead position z centered above the sensor:

$$U_{\mathrm{Hall}} = \frac{S_I \cdot I_{\mathrm{meas}} \cdot \mu_0 \cdot \Delta m}{4\pi \left(z + z_0\right)^3}. \tag{1}$$

with S_I being the sensitivity, I_{meas} the current, μ_0 the magnetic permeability of the vacuum, Δm the magnetic moment of the bead, and z_0 the position offset. The fit of the data shown in Fig. 8(a) results in $z_0 = 2.06$ μm which corresponds well to the sum of the bead radius (1.4 μm) and the sensor thickness measured by atomic force microscopy (660 nm). A Langevin coefficient $\alpha = 0.95$ Am^2 J^{-1} was found, corresponding to a magnetic susceptibility χ= 0.6 of the bead. The spatial sensitivity for our sensors is shown in Fig. 8(b) [derivative of (1)] and its maximum value was about 1 μV/μm at 0 nm distance, decaying with z^{-4} to zero.

The corresponding spatial resolution is 230 nm(Hz)$^{-1/2}$ with an inductive noise limit of 100 nV (which would reduce to 23 nm(Hz)$^{-1/2}$ for the noise limit of 10 nV in the absence of the parasitic inductive signal). The Hall sensor thermal noise limit of about 1 nV(Hz)$^{-1/2}$ would correspond to a spatial resolution of better than 1 nm(Hz)$^{-1/2}$.

V. Conclusion and Outlook

We have demonstrated superparamagnetic bead detection with the FEB-deposited Hall sensors. They consist of tunable metal-matrix nanocomposite material which can be downscaled to at least 100 nm active area size without losing magnetic detection properties. An original SEM-integrated method was developed that allows measuring directly sensor sensitivity by moving the bead precisely above the sensor by nanomanipulation.

For the dynamic and static detection schemes reported in this paper, the magnetic field and spatial resolutions are presently limited by at least one order of magnitude due to the large parasitic inductive voltage of about 1 mV. This can be overcome by compensating the flux loops in the printed circuit board design or by using on-chip integrated current lines [38] to locally generate magnetic fields that will polarize and magnetically guide the beads inside microfluidic channels in lab-on-chip devices.

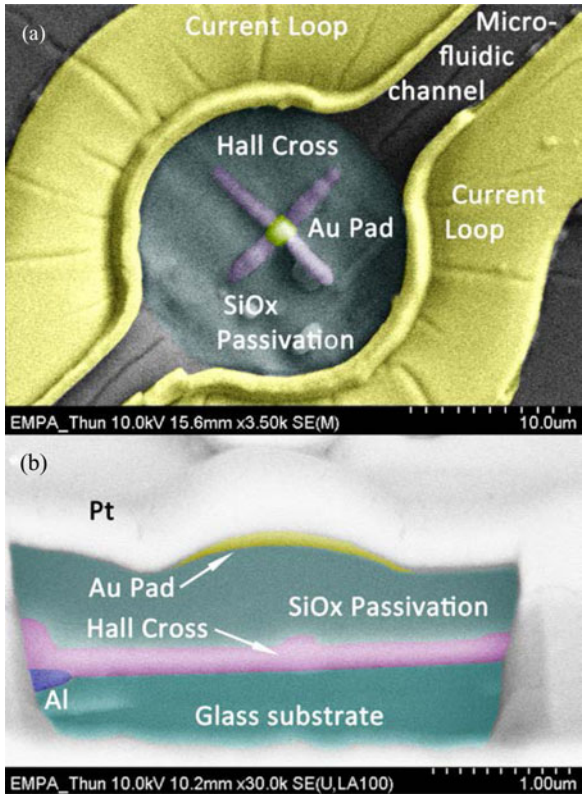

Fig. 9. (a) Top-view SEM image of a FEBID-integrated Hall sensor into a microfluidic platform from Chaves *et al*. [25]. (b) The 65° tilt FIB cross section shows three FEBID deposited materials: 1) the cobalt–carbon nanocomposite material of the Hall sensor connecting to the prefabricated aluminum electrode; 2) the SiO_x passivation material; and 3) the gold–carbon pad. The glass substrate and the platinum protection layer for the FIB cut are also seen.

To prove the Hall sensor integration into lab-on-chip devices by FEBID, we used the microfluidic platform which was developed for magnetoresistive sensors on glass substrates by Chaves *et al*. [25]. It consists of a 4.5 μm deep microfluidic channel in photoresist with current loops of gold which generate a magnetic field and aluminum electrodes to connect to the electronics periphery, see Fig. 9(a) and (b). In the final operative lab-on-chip device, the magnetic field would pull a superparamagnetic bead, fixed by a DNA to the sensor, upward and straighten the DNA; any height changes which occur due to antigen–antibody triggered restriction enzymes curling up the DNA will be sensed by the sensor.

Due to its minimally invasive nature, FEBID could be performed as a single postprocess step directly on the microfluidic platform. Fig. 9 shows the Co–C Hall cross connecting to the electrodes, an SiO_x capping layer, and a gold pad, all directly written by FEBID using $Co_2(CO)_8$, tetraethylsiloxane, and dimethyl-gold-trifluoroacetylacetonate as precursors, respectively. The SiO_x capping layer (thickness 350 nm) serves as sensor passivation against the liquid. Its thickness needs to be thinner than 1.8 μm to assure a good Hall sensor sensitivity, see Fig. 8(b). The thin gold pad (80 nm) on top of the sensor area allows for grafting of biological material, like DNAs via

thiolization. The thickness of any of the FEBID layers can be individually tuned by changing the beam exposure time. The sensor characterization on this platform is in progress.

ACKNOWLEDGMENT

The authors would like to thank R. Chaves and P. Freitas from Instituto de Engenharia de Sistemas e Computadores-Microsistemas e Nanotecnologias, Portugal, for providing their microfluidic platform and acknowledge fruitful discussions with them, and O. Kazakova and K. Firman in the frame of the EU BioNanoSwitch project (www.bionano-switch.info/).

REFERENCES

[1] B. Abeles, P. Sheng, M. D. Coutts, and Y. Arie, "Structural and electrical properties of granular metal films," *Advances Phys*., vol. 24, pp. 407–461, 1975.

[2] D. L. LesliePelecky and R. D. Rieke, "Magnetic properties of nanostructured materials," *Chemistry Mater*., vol. 8, pp. 1770–1783, Aug. 1996.

[3] A. B. Pakhomov, X. Yan, and B. Zhao, "Giant Hall effect in percolating ferromagnetic granular metal-insulator films," *Appl Phys. Lett*., vol. 67, pp. 3497–3499, 1995.

[4] L. Serrano-Ramón, R. Córdoba, L. A. Rodríguez, C. Magén, E. Snoeck, C. Gatel, I. Serrano, M. R. Ibarra, and J. M. De Teresa, "Ultrasmall functional ferromagnetic nanostructures grown by focused electron-beam-induced deposition," *ACS Nano*, vol. 5, pp. 7781–7787, 2011.

[5] A. Sandhu, A. Okamoto, I. Shibasaki, and A. Oral, "Nano and micro Hall-effect sensors for room-temperature scanning Hall probe microscopy," *Microelectron. Eng*., vol. 73–4, pp. 524–528, Jun. 2004.

[6] G. Mihajlovic, P. Xiong, S. von Molnar, M. Field, G. J. Sullivan, K. Ohtani, and H. Ohno, "Submicrometer Hall sensors for superparamagnetic nanoparticle detection," *IEEE Trans. Magn*., vol. 43, no. 6, pp. 2400–2402, Jun. 2007.

[7] J. Moritz, B. Rodmacq, S. Auffret, and B. Dieny, "Extraordinary Hall effect in thin magnetic films and its potential for sensors, memories and magnetic logic applications," *J. Phys. D-Appl. Phys*., vol. 41, pp. 135001-1–135001-8, Jul. 2008.

[8] M. S. Gabureac, L. San Emeterio Alvarez, and C. H. Marrows, "Co/Pt Hall sensors for low field detection," *Procedia Chemistry*, vol. 1, pp. 851–854, 2009.

[9] P. P. Freitas, R. Ferreira, S. Cardoso, and F. Cardoso, "Magnetoresistive sensors," *J. Phys.: Condensed Matter*, vol. 19, pp. 165221-1–165221-21, 2007.

[10] I. Utke and A. Gölzhäuser, "Small, minimally invasive, direct: Electrons induce local reactions of adsorbed functional molecules on the nanoscale," *Angewandte Chemie – Int. Edition*, vol. 49, pp. 9328–9330, 2010.

[11] C. H. Schwalb, C. Grimm, M. Baranowski, R. Sachser, F. Porrati, H. Reith, P. Das, J. Müller, F. Völklein, A. Kaya, and M. Huth, "A tunable strain sensor using nanogranular metals," *Sensors*, vol. 10, pp. 9847–9856, 2010.

[12] J. Hyon Noh, M. Nikiforov, S. V. Kalinin, A. A. Vertegel, and P. D. Rack, "Nanofabrication of insulated scanning probes for electromechanical imaging in liquid solutions," *Nanotechnology*, vol. 21, pp. 365302-1–365302-10, 2010.

[13] M. G. Jenke, D. Lerose, C. Niederberger, J. Michler, S. Christiansen, and I. Utke, "Toward local growth of individual nanowires on three-dimensional microstructures by using a minimally invasive catalyst templating method," *Nano Lett*., vol. 11, pp. 4213–4217, 2011.

[14] F. De Angelis, G. Das, P. Candeloro, M. Patrini, M. Galli, A. Bek, M. Lazzarino, I. Maksymov, C. Liberale, L. C. Andreani, and E. Di Fabrizio, "Nanoscale chemical mapping using three-dimensional adiabatic compression of surface plasmon polaritons," *Nature Nanotechnol*., vol. 5, pp. 67–72, 2010.

[15] H. C. George, T. A. Orlova, A. O. Orlov, and G. L. Snider, "Novel method for fabrication of nanoscale single-electron transistors: Electron beam induced deposition of Pt and atomic layer deposition of tunnel barriers," *J. Vacuum Sci. Technol. B*, vol. 29, pp. 06fb01-1–06fb01-4, Nov. 2011.

[16] M. Gavagnin, H. D. Wanzenboeck, D. Belić, and E. Bertagnolli, "Synthesis of individually tuned nanomagnets for nanomagnet logic by direct write focused electron beam induced deposition," *ACS Nano*, vol. 7, pp. 777–784, 2013.

[17] I. Utke, M. G. Jenke, C. Röling, P. H. Thiesen, V. Iakovlev, A. Sirbu, A. Mereuta, A. Caliman, and E. Kapon, "Polarisation stabilisation of vertical cavity surface emitting lasers by minimally invasive focused electron beam triggered chemistry," *Nanoscale*, vol. 3, pp. 2718–2722, 2011.

[18] C. Danelon, C. Santschi, J. Brugger, and H. Vogel, "Fabrication and functionalization of nanochannels by electron-beam-induced silicon oxide deposition," *Langmuir*, vol. 22, pp. 10711–10715, 2006.

[19] M. Huth, "Granular metals: From electronic correlations to strain-sensing applications," *J. Appl. Phys*., vol. 107, pp. 113709-1–113709-7, 2010.

[20] M. S. Gabureac, L. Bernau, I. Utke, J. M. deTeresa, and A. Fernandez-Paccheco, "Focused ion and electron beam induced deposition of magnetic nanostructures," in *Nanofabrication Using Focused Ion and Electron Beams: Principles and Applications*, I. Utke, S. Moshkalev, and P. Russel, Eds. New York, NY, USA: Oxford Univ. Press, 2013, p. 840.

[21] G. Boero, I. Utke, T. Bret, N. Quack, M. Todorova, S. Mouaziz, P. Kejik, J. Brugger, R. S. Popovic, and P. Hoffmann, "Submicrometer Hall devices fabricated by focused electron-beam-induced deposition," *Appl. Phys. Lett*., vol. 86, pp. 042503-1–042503-3, 2005.

[22] T. Lionnet, S. Joubaud, R. Lavery, D. Bensimon, and V. Croquette, "Wringing out DNA," *Phys. Rev. Lett*., vol. 96, pp. 178102-1–178102-4, May 2006.

[23] R. Seidel and C. Dekker, "Single-molecule studies of nucleic acid motors," *Current Opinion Structural Biology*, vol. 17, pp. 80–86, 2007.

[24] I. M. Hsing, Y. Xu, and W. Zhao, "Micro-and nano-magnetic particles for applications in biosensing," *Electroanalysis*, vol. 19, pp. 755–768, 2007.

[25] R. C. Chaves, D. Bensimon, and P. P. Freitas, "Single molecule actuation and detection on a lab-on-a-chip magnetoresistive platform," *J. Appl. Phys*., vol. 109, pp. 064702-1–064702-8, 2011.

[26] L. Bernau, M. Gabureac, R. Erni, and I. Utke, "Tunable nanosynthesis of composite materials by electron-impact reaction," *Angewandte Chemie – Int. Edition*, vol. 49, pp. 8880–8884, 2010.

[27] M. S. Gabureac, L. Bernau, and I. Utke, "Nanosynthesis of tunable composite materials by room-temperature pulsed focused electron beam induced chemical vapour deposition," *J. Nanosci. Nanotechnol*., vol. 11, pp. 7982–7987, 2011.

[28] A. Candini, G. C. Gazzadi, A. Di Bona, M. Affronte, D. Ercolani, G. Biasiol, and L. Sorba, "Hall nano-probes fabricated by focused ion beam," *Nanotechnology*, vol. 17, pp. 2105–2109, May 2006.

[29] P. Vavassori, V. Metlushko, B. Ilic, M. Gobbi, M. Donolato, M. Cantoni, and R. Bertacco, "Domain wall displacement in Py square ring for single nanometric magnetic bead detection," *Appl. Phys. Lett*., vol. 93, pp. 203502-1–203502-3, Nov. 2008.

[30] M. Gabureac, L. Bernau, I. Utke, and G. Boero, "Granular Co-C nano-Hall sensors by focused-beam-induced deposition," *Nanotechnology*, vol. 21, pp. 115503-1–115503-5, Mar. 2010.

[31] P. A. Besse, G. Boero, M. Demierre, V. Pott, and R. Popovic, "Detection of a single magnetic microbead using a miniaturized silicon Hall sensor," *Appl. Phys. Lett*., vol. 80, pp. 4199–4201, Jun. 2002.

[32] G. Mihajlovic, P. Xiong, S. von Molnar, K. Ohtani, H. Ohno, M. Field, and G. J. Sullivan, "Detection of single magnetic bead for biological applications using an InAs quantum-well micro-Hall sensor," *Appl. Phys. Lett*., vol. 87, pp. 112502-1–112502-3, 2005.

[33] L. Ejsing, M. F. Hansen, A. K. Menon, H. A. Ferreira, D. L. Graham, and P. P. Freitas, "Planar Hall effect sensor for magnetic micro-and nanobead detection," *Appl. Phys. Lett*., vol. 84, pp. 4729–4731, Jun. 2004.

[34] O. Kazakova, J. C. Gallop, P. See, D. Cox, G. K. Perkins, J. D. Moore, and L. F. Cohen, "Detection of a micron-sized magnetic particle using InSb Hall sensor," *IEEE Trans. Magn*., vol. 45, no. 10, pp. 4499–4502, Oct. 2009.

[35] G. Mihajlović, K. Aledealat, P. Xiong, S. Von Molnár, M. Field, and G. J. Sullivan, "Magnetic characterization of a single superparamagnetic bead by phase-sensitive micro-hall magnetometry," *Appl. Phys. Lett*., vol. 91, pp. 172518-1–172518-3, 2007.

[36] G. Fonnum, C. Johansson, A. Molteberg, S. Mørup, and E. Aksnes, "Characterisation of Dynabeads® by magnetization measurements and mössbauer spectroscopy," *J. Magnetism Magn. Mater.*, vol. 293, pp. 41–47, 2005.

[37] M. Megens, F. De Theije, B. De Boer, and F. Van Gaal, "Scanning probe measurements on a magnetic bead biosensor," *J. Appl. Phys*., vol. 102, pp. 014507-1–014507-5, 2007.

[38] Y. Kumagai, K. Togawa, S. Sakamoto, M. Abe, H. Handa, and A. Sandhu, "Hall biosensor with integrated current microstrips for control of magnetic beads," *IEEE Trans. Magn*., vol. 42, no. 12, pp. 3893–3895, Dec. 2006.

Authors' photographs and biographies not available at the time of publication.